N89-22168

AN ASSESSMENT OF AVIRIS DATA FOR HYDROTHERMAL ALTERATION MAPPING IN THE GOLDFIELD MINING DISTRICT, NEVADA

VERONIQUE CARRERE and MICHAEL J. ABRAMS, Jet Propulsion Laboratory, California Institute of Technology, Pasadena, CA 91109

ABSTRACT

Airborne Visible and Infrared Imaging Spectrometer (AVIRIS) data were acquired over the Goldfield Mining District, Nevada, in September 1987. Goldfield is one of the group of large epithermal precious metal deposits in Tertiary volcanic rocks, associated with silicic volcanism and caldera formation. Hydrothermal alteration consists of silicification along fractures, advanced argillic and argillic zones further away from veins and more widespread propylitic zones. Alteration minerals include alunite, kaolinite, adularia and opal, montmorillonite and chlorite. An evaluation of AVIRIS data quality (spectral accuracy, signal to noise performance, signal variations,...) was performed. Faults in the data, related to engineering problems and a different behaviour of the instrument while on-board the U2, were encountered. Consequently, a decision was made to use raw data and correct them only for dark current variations and detector read-out-delays. New software was written to that effect. Atmospheric correction was performed using the "flat field" correction technique. Analysis of the data was then performed to extract spectral information, mainly concentrating on the 2-2.45 micron window, as the alteration minerals of interest have their distinctive spectral reflectance features in this region. Principally kaolinite and alunite spectra were clearly obtained. Mapping of the different minerals and alteration zones was attempted using ratios and clustering techniques. Poor signal-to-noise performance of the instrument and the lack of appropriate software prevented us from producing an alteration map of the area. Spectra extracted locally from the AVIRIS data were checked in the field by collecting representative samples of the outcrops. In all cases, lab PIDAS (Portable Instant Display and Analysis Spectrometer) and Beckman UV5240 measurements verified the identifications obtained from AVIRIS data. Despite the rather poor quality of the data and the lack of appropriate software, this test demonstrates the potential of high resolution imaging spectrometers for alteration mapping and identification of mineralogy.

I. INTRODUCTION

This paper describes some preliminary results arising from the analysis and interpretation of data from the September 1987 Airborne Visible and Infrared Imaging Spectrometer (AVIRIS) flight over Goldfield Mining District, Nevada.

AVIRIS acquires simultaneously 224 channels (distributed over 4 spectrometers) of data in the 0.4 to 2.45 micron region, with an average spectral resolution of about 10 nm. Operating from NASA's U2 at an altitude of 20 km, the IFOV is 20m with a swath width of 12 km. This is the first instrument of its kind to obtain complete high spectral resolution reflectance data with a wide swath width.

The Goldfield Mining district was selected as a test area because it is one of a group of large epithermal precious-metal deposits in Tertiary volcanic rocks found in the western part of the Great Basin. The area covered by the AVIRIS flight includes the eastern part of the Goldfield Hills (Figure 1). Study of the data focused on the main alteration area. Formations represented in the test-area are mainly Miocene in age. They are composed of pyroclastic tuffs and welded ash flow tuffs of early Miocene age (about 22-20.5 M.Y old, Ashley and Silbermann, 1976; Cornwall, 1972), ranging in composition from dacitic to quartz latitic and rhyolitic. Lava flows and intusives of similar composition and some andesites and basalts are also common.

The oldest most widespread and most voluminous of these units is the Milltown Andesite, which consists of trachyandesite and rhyodacite tuffs and flows with minor basalts and quartz latite. A K-Ar age of 21.5 M.Y makes the formation Miocene in age (Silbermann and MacKee, 1972).

A porphyritic rhyodacite (unnamed dacite of Ransome, 1909) intrudes and overlies the Milltown Andesite, forming a group of flow dome complexes. These rocks are particularly prominent in the test area. The sequence includes localized units of quartz latite, andesite and basalt.

The Milltown Andesite and porphyritic rhyodacite are overlain by the Tuff of Chispa Hills (unnamed dacite vitrophyre of Ransome, 1909) and the Chispa andesite, a trachyandesite flow, on the south side of the area, and by the andesite-rhyodacite breccia on the eastern side. The andesite-rhyodacite breccia is a locally very coarse breccia sheet, composed of debris from the Milltown Andesite and porphyritic rhyodacite.

The Spreadhead Member of the Thirsty Canyon Tuff flanks the Goldfield Hills on the south side of the area. It consists of a sequence of rhyolitic to pantelleritic ash flow and minor ash-fall tuffs that were erupted from the Blackcap Mountain caldera area. The Thirsty Canyon Tuff and associated lavas are Pliocene in age (Noble and others, 1964).

Three major structural events happened in this area. Ashley (1972) suggested that the oldest tertiary structure in the district is a ring fracture. Faulting occurred during the period of early Miocene volcanism. The faulting and mineralization were probably both produced by a pluton that intruded the area to shallow levels but did not reach the surface. The test-area is mainly affected by

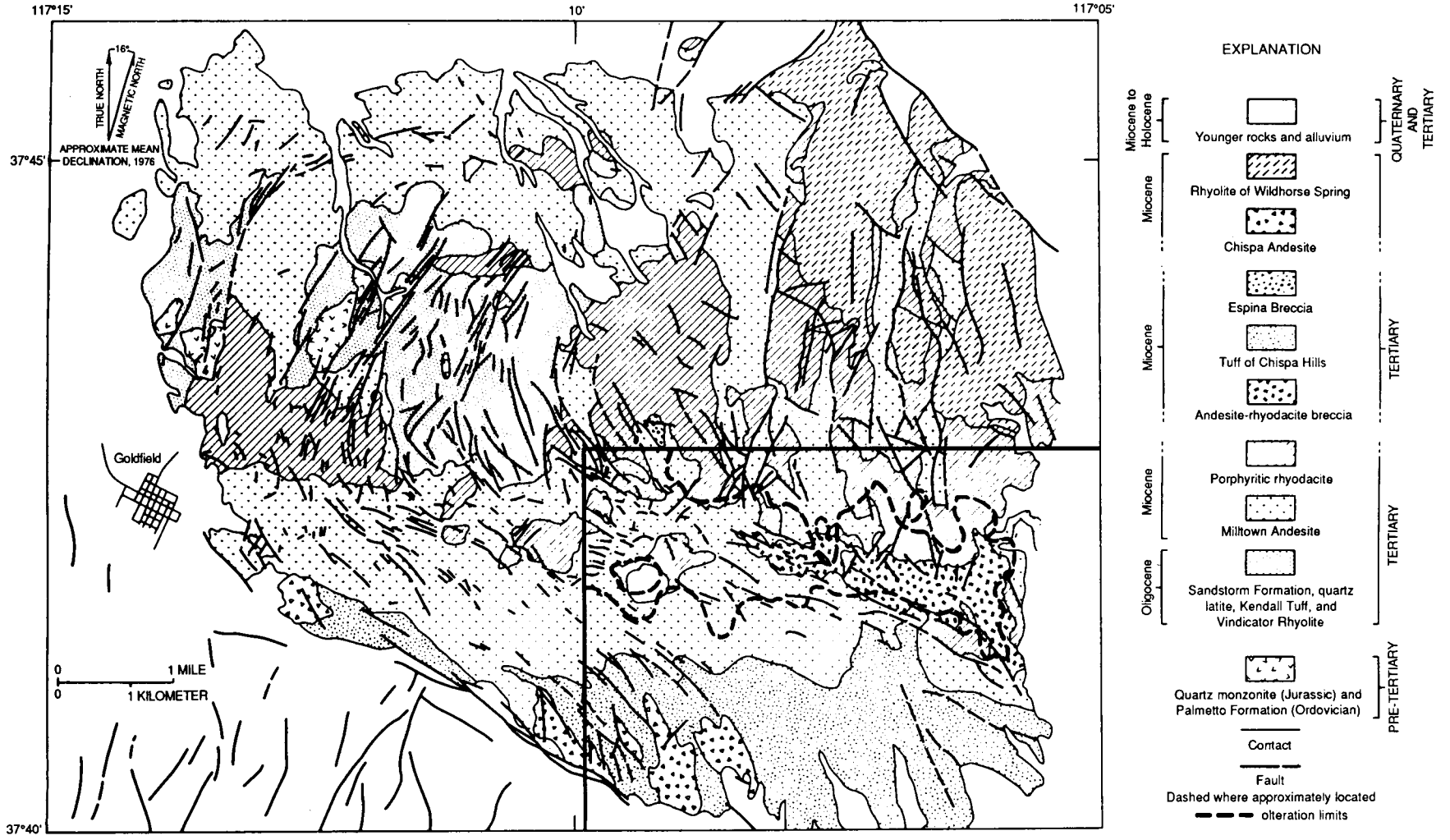

FIGURE 1. Generalized geologic and alteration map of the Goldfield Mining District (after Ashley, 1976) Location of the study area.

late Tertiary faults (Basin and Range faults), mostly northerly trend and NW trending post-Siebert faults.

Hydrothermal alteration and ore deposition at Goldfield occured within the episode of andesitic-dacitic volcanism beginning with the Milltown Andesite and ending with the Chispa Andesite. Although the Milltown Andesite, porphyritic rhyodacite, andesite-rhyodacite breccia and Tuff of Chispa Hills are hydrothermally altered, the Chispa Andesite is not.

Direct dating of hydrothermal minerals (alunite and sericite) yield an age range of 21-20 MY for the hydrothermal alteration (Ashley and Silbermann, 1976). Alteration zones (Table 1) include silicified zones along fractures, many alunite-bearing, surrounded by advanced argillic, argillic and more widespread propylitic zones (Harvey and Vitaliana, 1964; Ashley and Albers, 1975; Ashley, 1974). Some montmorillonite-bearing argillic areas also occur.

Table 1

ALTERATION TYPE	MAJOR MINERALS
Silicified	Q+Al+K+Pp+D+Km
Advanced Argillic	Q+Al+Pp+K+D+Op+Km
Argillic	Q+K+Km+mixed layers
Montmoril.-bearing Argillic	M+K+Q+mixed layers+Ca+Chl
Propylitic	Ep+Chl+Ab+Ca+minor K-mica and Pyrite

ABBREVIATIONS:				
	Ab	Albite	K	Kaolinite
	Al	Alunite	Km	K-mica
	Ca	Calcite	M	Montmorillonite
	Chl	Chlorite	Op	Opal
	D	Diaspore	Pp	Pyrophyllite
	Ep	Epidote	Q	Quartz

The basic objective of this study was to determine the efficiency of AVIRIS data for hydrothermal alteration mapping. An evaluation of the intrinsic properties of the instrument during its September 14th overflight of Goldfield was also performed.

After being corrected for dark current variations, detector read-out delays and atmospheric effects, various techniques were applied to identify minerals using spectral information, and map alteration zones using mineral assemblage and distribution. Since most of the minerals involved in the alteration process present features in the near-infrared, the study focused on the 2.0-2.45 micron region (see table 2).

Results were checked by collecting samples in the field and getting lab PIDAS (Portable Instant Display and Analysis Spectrometer) and Beckman UV5240 spectra. Mainly kaolinite and alunite were identified but the quality of the data and the lack of appropriate software prevented us from mapping alteration zones.

Table 2

MINERAL	ABSORPTION FEATURES (microns)
Alunite	1.77; 2.17; 2.20; 2.317
Calcite	2.34
Chlorite	2.26; 2.355
Kaolinite	2.16; 2.21
K-mica	2.205; 2.3; 2.4
Montmorillonite	2.2
Pyrophyllite	2.166; 2.314

II. DATA QUALITY

Some problems, related to AVIRIS data acquisition have been brought to our attention while evaluating our data set.

1. Drift in the offset

The most serious is that the instrument offset, particularly in spectrometer D, is subject to long term drift. This results in a lower or higher than optimum offset and, in the worst case, data clipping. It shows up in the data as detector elements having apparent outputs of zero (Figure 2). This drift was related to:
-the poor quality of the potentiometers used in the pre-amplifier circuits to adjust offset magnitude (Vane, personal communication);
-changes in temperature; it has been noticed that small changes in the detector temperature could give rise to offset signals equal to the predicted full scale image signal (Steinkraus and Hickok, 1987). This can be explained by the fact that the spectrometer heater configuration designed to athermalize the spectrometers and thereby maintain alignment of the optical elements was not adequate for the U2 flight environment (Vane, personal communication);
-nonsystematic vibration introducing fluctuation in instrument output level.

2. Offset in brightness

An offset in brightness occurs in the middle of the scene. This is also the result of a vibrationally induced change in the potentiometer setting in a pre-amplifier circuit which caused a step change in the offset applied to the data during onboard processing.

3. Noise characterization

Several types of noise are present in the data. First, an estimation of the signal-to-noise performances of the instrument for this data set was done. Two methods were used. The first one (Figure 3) consists in calculating the mean spectral response of an homogeneous area and its standard deviation (Conel et al., 1987).

The mean value of the average response is considered to be the signal and the noise estimate is provided by the standard deviation. The ratio mean/standard deviation gives a first estimation of the signal-to-noise response for each wavelength. The only homogeneous area big enough to be used in the scene was the Chispa Andesite which happens to be dark. But using a 9x9 area increases the signal-to-noise and partly compensates for this problem. According to this method, the signal-to-noise in the various spectrometers is (Figure 4):

A 30/1
B 10/1
C 10/1
D 8/1

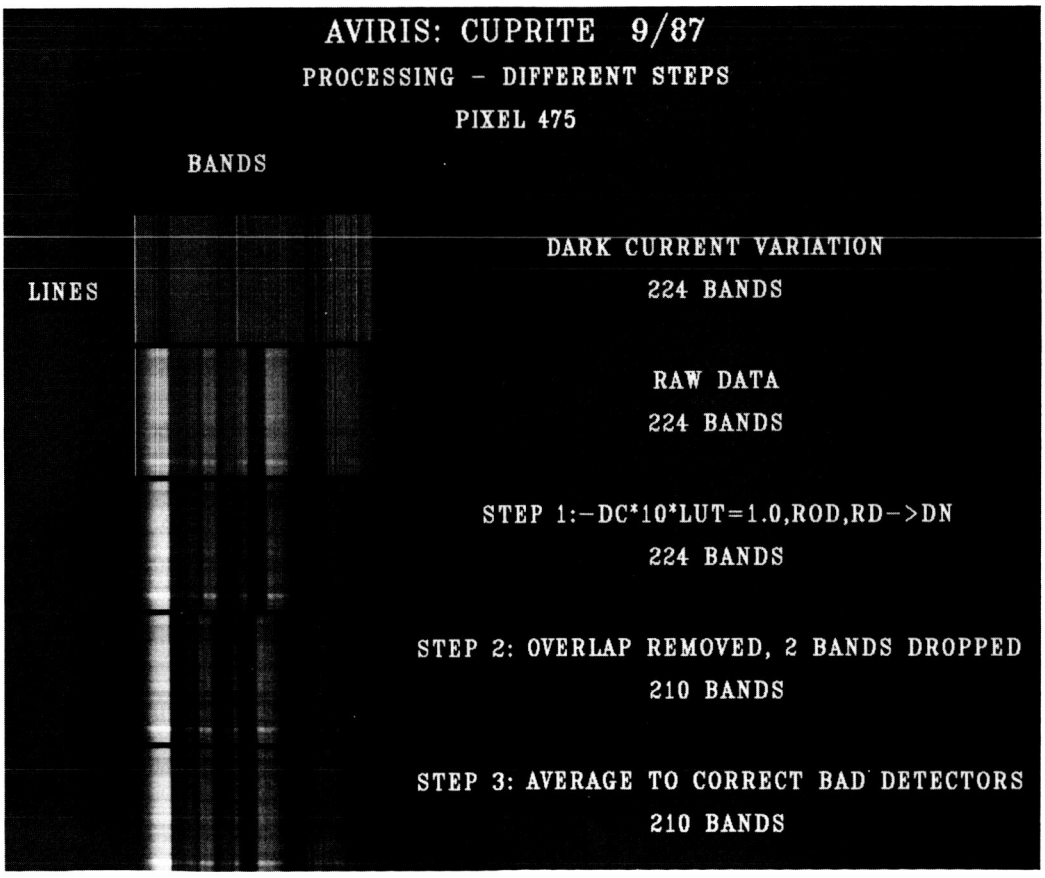

Figure 2. Different steps used to pre-process the AVIRIS data

A second way to estimate the quantity of noise in the data coming from the instrument itself and allowing us to get rid of any inhomogeneity in the data is to look at the standard deviation of the dark current (Figure 5). By dividing the signal coming from one single pixel by the standard deviation of the average dark current, we get another estimation of the signal-to-noise. This has been done for a bright sample and a dark sample to give an idea of the range.

The results are (Figure 6):

A	30:1 to 70:1
B	10:1 to 30:1
C	10:1 to 25:1
D	8:1 to 18:1

Both methods give consistent results. The second one presents the advantage of characterizing the instrument itself and should be more accurate.

A quick comparison (Table 3) with the performances published before the flight season shows that, even in the best case (bright sample), the noise level increased drastically.

The image data also contain periodic noise and, at least, three distinct spatially recognizable patterns are present. The most prominent of these has a period of about 10.3 lines per cycle (0.097 line-1) normal to the banding, which trends at an angle of about 18 degrees to the scan direction. A second band set has a period of 12.8 lines per cycle (0.78 line-1) at an angle of about 65 degrees; the third periodic variation is manifested within the second set with a period of one line per cycle (1 line-1) along the flight direction.

Table 3

SPECTROMETER	1st METHOD	2nd METHOD	LAB (pre-flight)
A	30:1	30:1-70:1	151:1
B	10:1	10:1-30:1	140:1
C	10:1	10:1-25:1	70:1
D	8:1	6:1-18:1	30:1

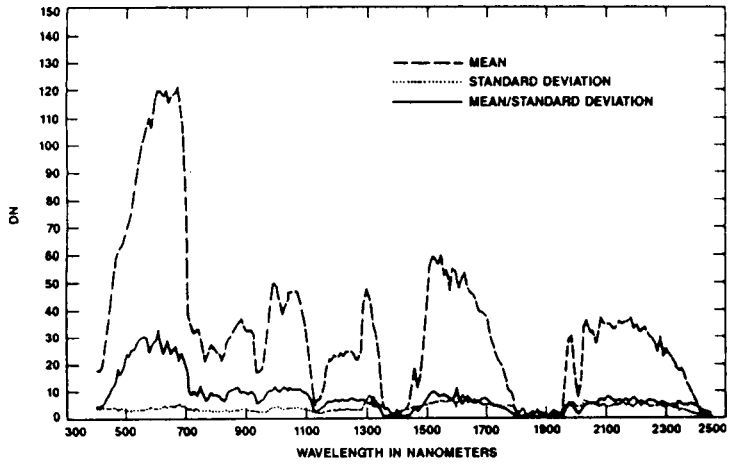

FIGURE 3. Estimation of signal-to-noise (method n°1)

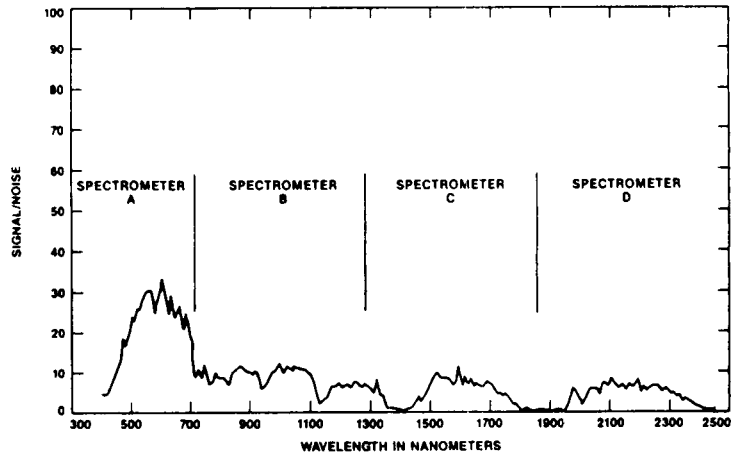

FIGURE 4. Signal-to-noise results from method n°1

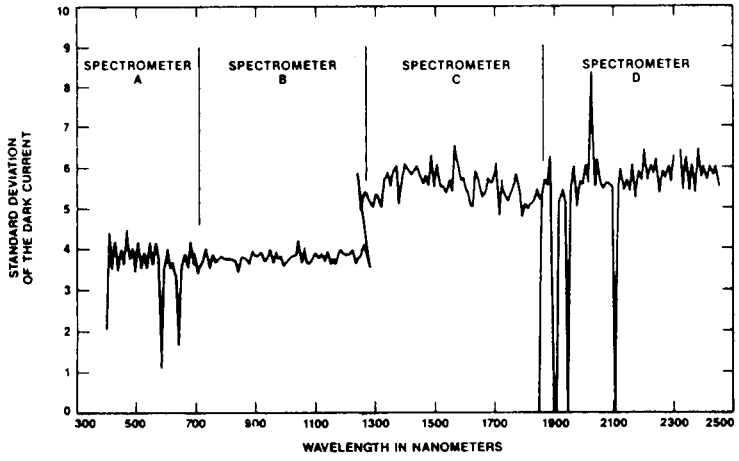

FIGURE 5. Estimation of the noise (method n°2)

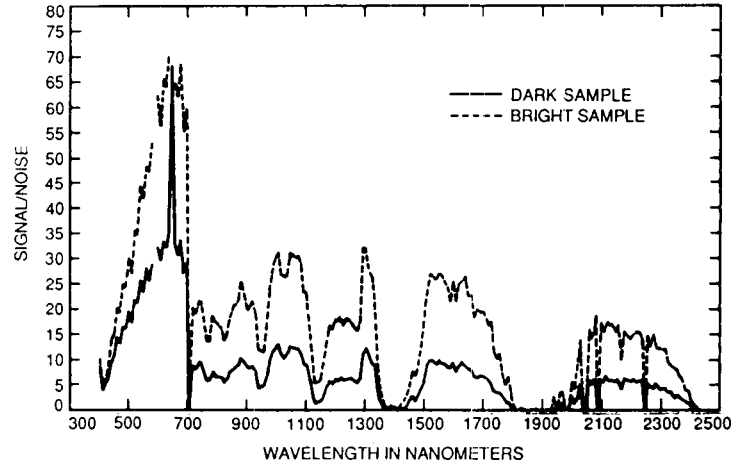

FIGURE 6. Signal-to-noise range (method n°2)

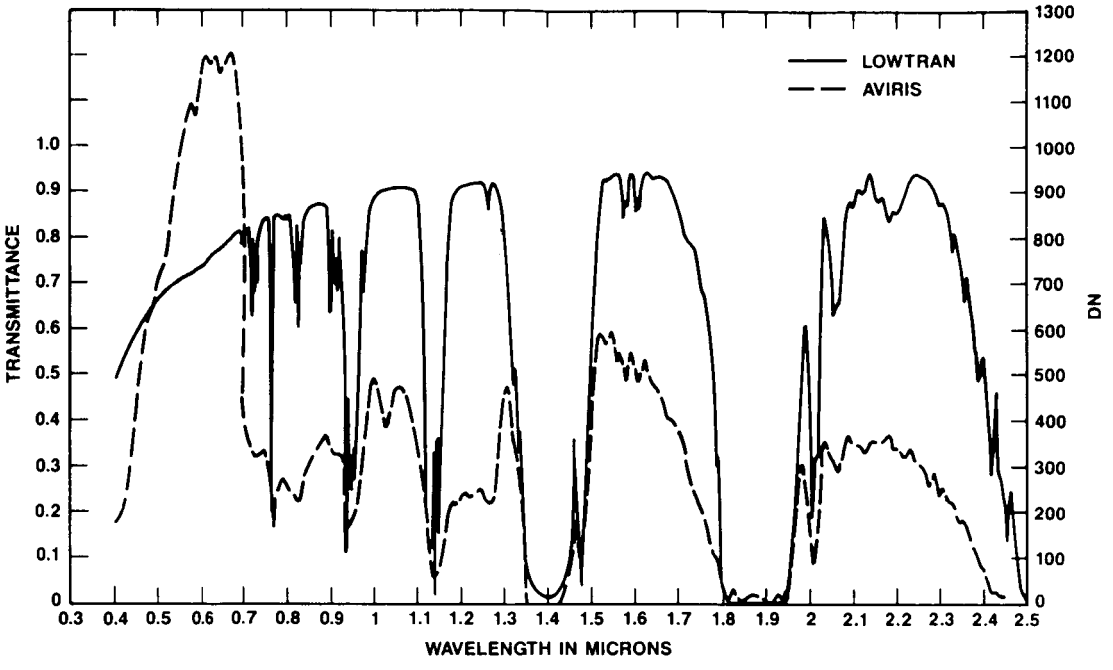

Figure 7. Estimation of the Effective Spectral Resolution

The precision oscillator has been identified as one possible part of the problem of increase of the level of random noise by a factor of two in spectrometer D. Mechanical vibrations of the circuit boards and their components seem to be responsible for the rise of fixed pattern noise in spectrometer D.

After termination of the flight season, inspection revealed that the optical fibers connecting spectrometer A and B to the foreoptics had come loose from their mountings. This can explain the loss of 50% signal caused by the resulting defocusing.

4. Estimation of effective inflight spectral resolution

A quick estimation of the inflight spectral resolution was performed. By spectral resolution, we mean the detection of separate radiance minima associated with neighboring absorption bands. We chose to compare the AVIRIS raw spectrum of the same homogeneous area and the model for the atmospheric transmittance provided by LOWTRAN 7. Figure 7 shows a perfect match between the atmospheric absorption bands displayed by AVIRIS and those from LOWTRAN. This means that the sampling interval is correct and that sharp features can be resolved by AVIRIS. For example, the pair of CO2 bands at 2050nm (in spectrometer D) are clearly resolved. A more detailed study of these characteristics can be found in Green and Vane (1988). It shows that the spectral resolution (or sampling interval) is of about 10nm in spectrometers C and D and about 20 nm in spectrometers A and B.

5. Summary

Data characteristics can be summarized as follows:

1. As a consequence of a drift in the offset, several detector elements have an apparent response of zero, particularly in spectrometer D.

2. The signal-to-noise performances are by far lower than those announced before the flight season, mainly because of engineering problems and a different behaviour of the instrument while on board the U2.

3. The spectral resolution seems to be as good as expected.

III. DATA CORRECTION

Trying to map alteration using mineral spectral absorption features generally implies using calibrated data and radiance to be able to compare them easily with lab or field spectral measurements. The standard procedure used at JPL to calibrate AVIRIS data (see, Reimer, 1988) includes:

- dark current subtraction,
- conversion to radiance using a calibration file obtained on lab (see, Chrien, 1988),
- detector read-out delays correction (spatial resampling),
- spectral resampling using interpolation, ending up with 210 bands and a sampling interval of 9.8nm.

Considering the problems presented previously, it did not seem appropriate:

1. to transform the data into radiance using a calibration file that does not reflect the state of the instrument on board the U2. As the calibration file is a multiplicative factor, it will disappear anyway when correcting the data for atmospheric effects using flat field correction or normalization technique.
2. to proceed with a spectral resampling which would include detector elements showing an apparent output of zero and spread those wrong values.

So the procedure was modified to perform only dark current subtraction and detector read-out delays correction. The "clipped" detectors were replaced by the average value of the previous and next element. The overlap between spectrometers was removed and two bands were dropped in spectrometer B (as no specific absorption features for interesting minerals occur in that portion of the spectrum) to end up with the 210 bands. No spectral resampling was performed as the sampling intervals for each spectrometer are close enough (9.56 to 10nm)(see Figure 3).

The offset in brightness was corrected by subtracting the dark current separately from each part.

Retrieval of ground reflectance

Easy to apply methods of compensating for the atmosphere, not requiring radiometric calibrated data, are available. The most common one is the "flat spectral field reduction". This correction procedure involves formation of ratio of the radiance from an unknown target to the radiance of a standard target whose spectral reflectance is known or independant of wavelength.

To implement the flat-field procedure, we used the Chispa Andesite as the reference as it is the only spectrally flat formation available in the scene. It is dark, homogeneous and unaltered. A 9x9 area was used to compensate for the waste of signal-to-noise due to the use of a dark area. The entire scene was divided by this average spectrum.

The only inconvenience of this method is that it does not compensate for path radiance, which can be a problem in the visible, resulting in shift in wavelength for some features. LOWTRAN model can be used to make an approximate correction (Conel et al., 1987), but as we were focussing on the 2.0-2.45 portion of the spectrum, we decided not to do it.

The normalization technique was also used, that is to say dividing the entire scene by the average spectrum of the entire flight line. This procedure did not give results as good as the flat-field correction technique, presumably because of too-important spectral variations and elevation changes in the scene.

IV. DATA ANALYSIS

1. Local analysis

Spectra were first extracted locally to check if, despite the low signal-to-noise, minerals could be identified and discriminated. Areas were picked refering to an AVIRIS color composite of the test-site (Figure 8) and geologic maps.

Several spectra, corresponding to an average of 9 to 15 samples (Figures 9 and 10), mainly showing kaolinite and alunite absorption features, were obtained using VICAR and CSIRO software. It seemed at that point that minerals involved in hydrothermal alteration, as they generally display deep absorption bands, could be identified.

2. Hydrothermal alteration mapping

The next step was to determine the spatial distribution of those minerals to end up with a map of the alteration zones. Different techniques were used: ratios, SPAM software, clustering.

a. Ratios

We first tried the classic method of ratioing, using the absorption features observed in the spectra extracted locally from the AVIRIS data themselves and theoretical values for the specific minerals we were looking for. Several combinations were

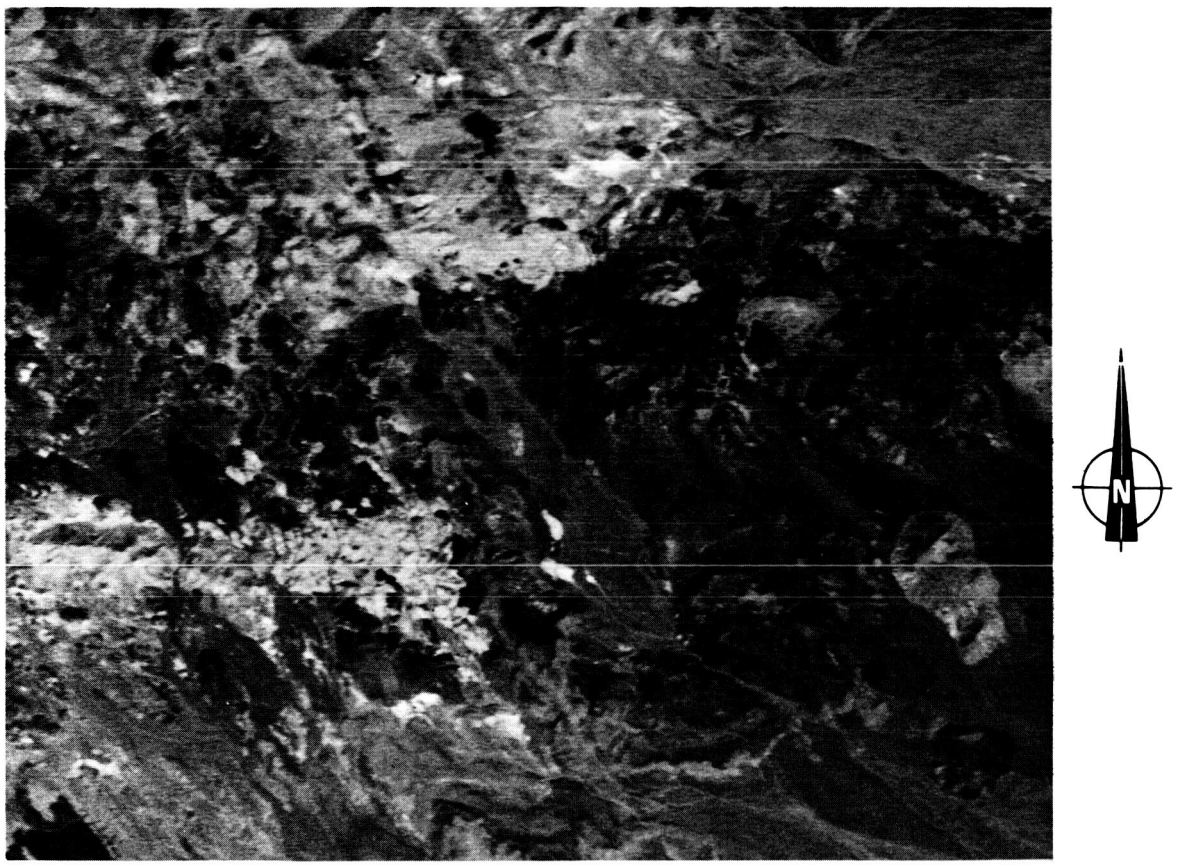

FIGURE 8. AVIRIS false-color composite of the test area (refer to slide No. 5). Red: b200 (2.21 μm); Green: b130 (1.56 μm); Blue: b50 (0.8 μm) (The bands are only corrected for dark current variations and detector read-out delays).

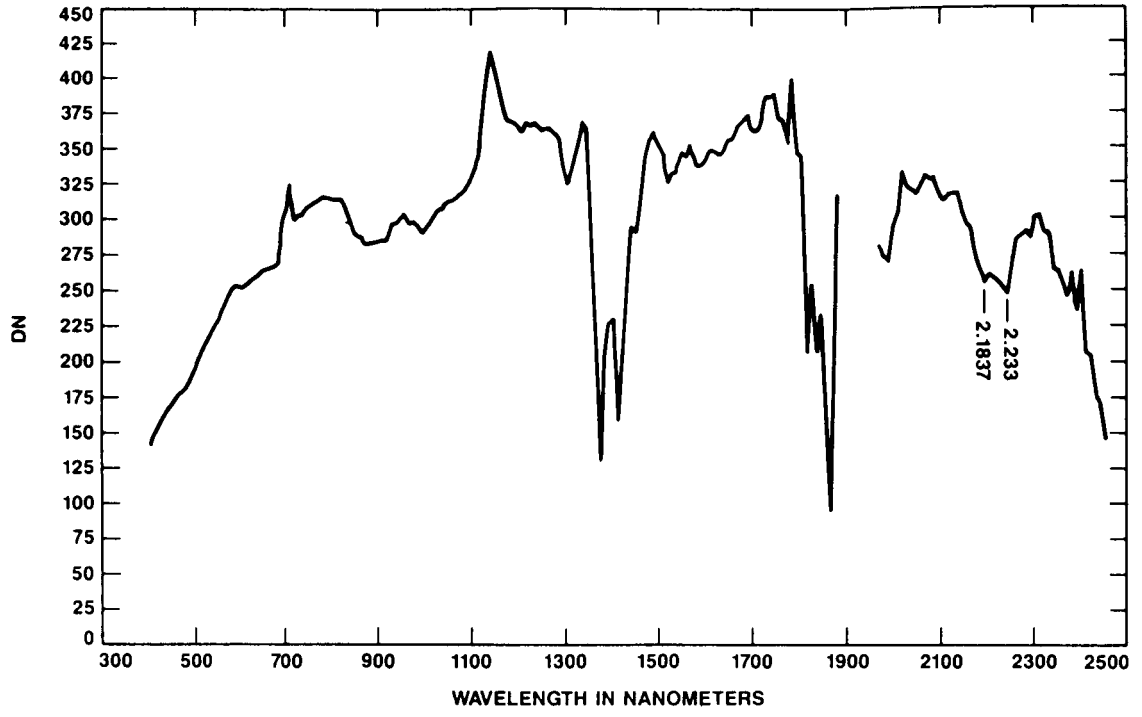

Figure 9: Example of spectrum extracted after flat-field correction (I)

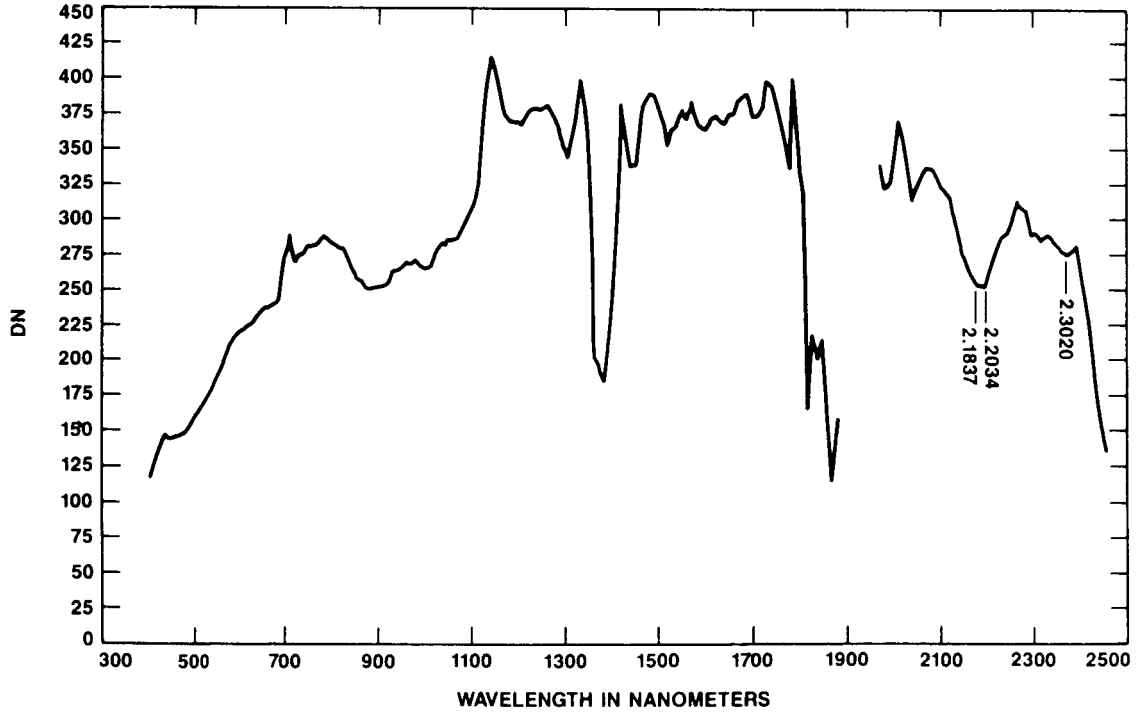

Figure 10: Example of spectrum extracted after flat-field correction (II)

tried. Results appeared noisy but showed color variations (Figure 11). The meaning of those different colors was checked by going back to the flat field corrected data and extracting the spectra corresponding to those areas. No clear relationship was found between specific colors and types of spectrum that could allow identification and mapping of minerals. This confirmed that the signal-to-noise performances of the instrument were not high enough to allow discrimination using this simple technique.

We tried to estimate roughly what were the chances to obtain a good ratio for kaolinite (Figure 12). The uncertainty on the continuum is given by:

$$\Delta c = \frac{\Delta noise}{c} = 6/63 = 9.5\%$$

The uncertainty on the feature is given by:

$$\Delta f = \frac{\Delta noise}{c} = 6/58 = 10.3\%$$

So, the uncertainty on the ratio is given by:

$$\Delta R = \sqrt{(\Delta c)^2 + (\Delta f)^2} = 14.06$$

According to this formula, there are 67% chances for the ratio to be in a range of ± 14.06%.

b. SPAM (Spectral Analysis Manager)

Knowing there was some information available at least locally, we tried to use a partly modified version of SPAM. We focused on the 2.0-2.35 portion of the spectrum and a 100x100 subarea as SPAM could not handle a complete AVIRIS data set at that time.

The spectra locally extracted during the first step were checked by comparing them to the spectra from the SPAM library. A good match was found in most of the cases (Figure 13).

We then tried to use the program "Cluster" to have an idea of which classes were present in the image and to what mineral or combination of minerals they could be related. It happened that this program was not working at that time so we tried next the program "Find", using our knowledge of the minerals that should be present in the area. It was impossible to get consistent results from this program. A decision was made to wait until the entire package has been checked and fixed.

As our goal was to get a map of the area, we tried to modify a clustering program already existing in TAE/VICAR2 so it can handle AVIRIS data.

C. Clustering

The program "CLUSAN" was modified to handle BIL data and 64 bands. This clustering algorithm uses the "simulated annealing"

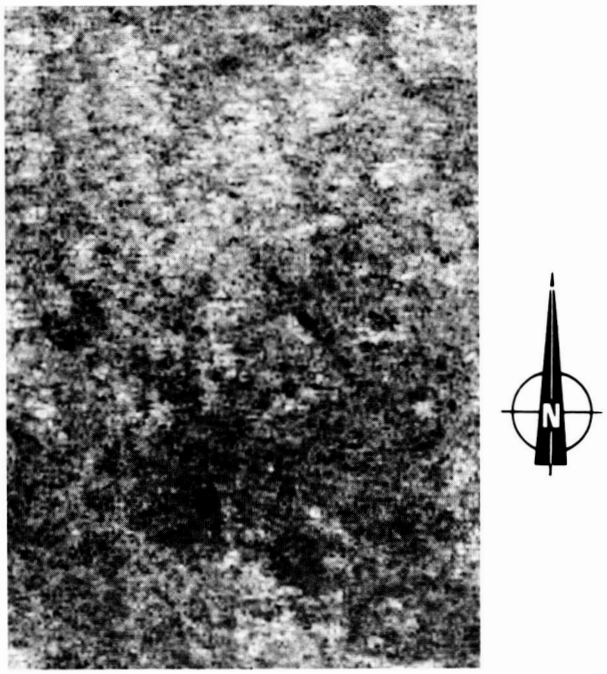

Figure 11: Example of color composite combining different ratios (refer to slide No. 6). Red: Kaolinite (b179/b172); Green: Jarosite (b5/b20); Blue: Alunite (b134/b131)

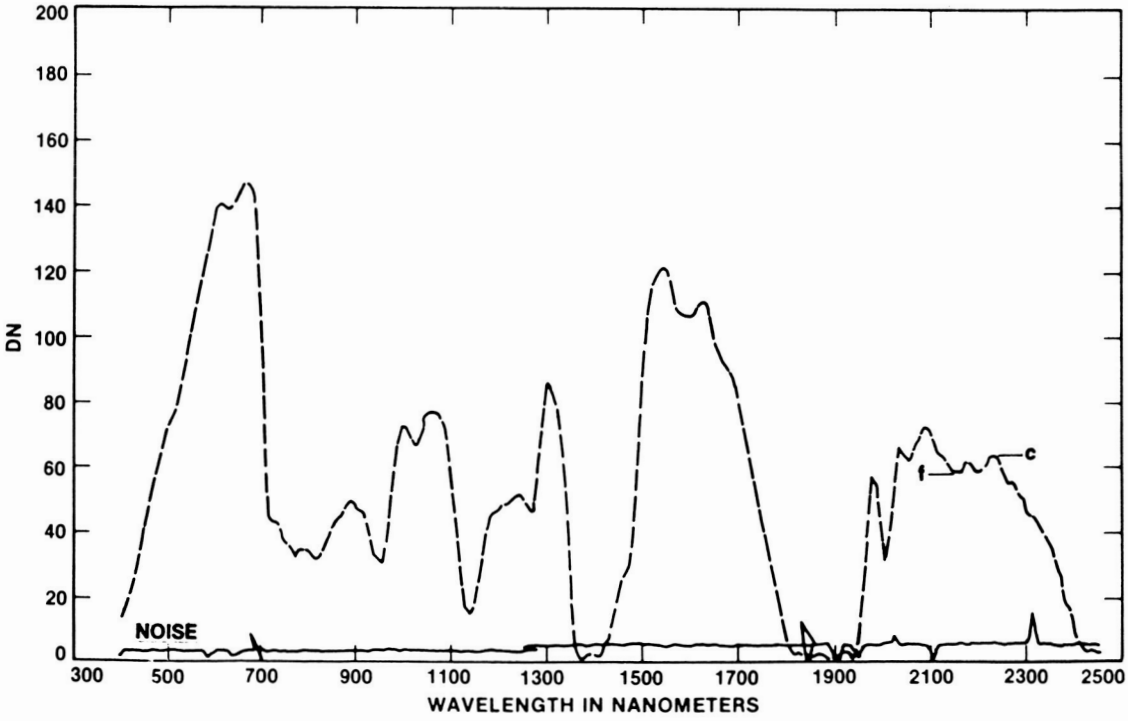

Figure 12: Estimation of ratioing efficiency-c: continuum; f: feature

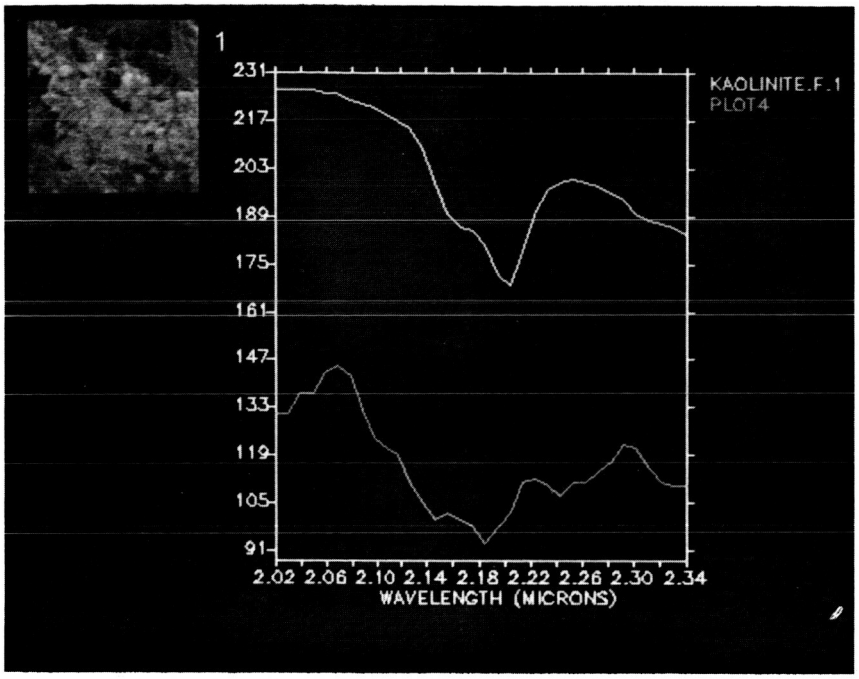

A

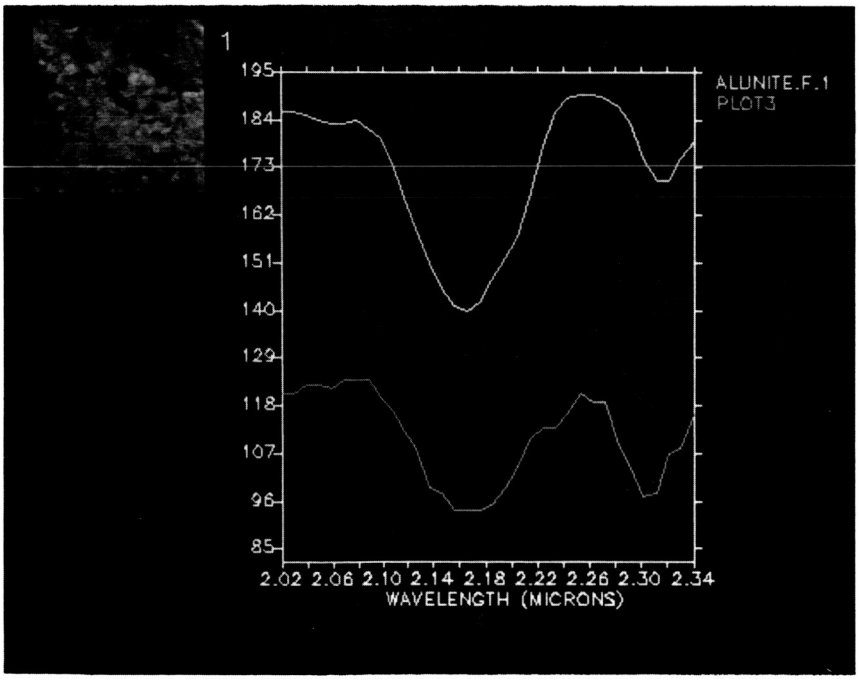

B

Figure 13: Comparison of AVIRIS spectra and library spectra using SPAM. A: Example of Kaolinite (refer to slide No. 7); B: Example of Alunite (refer to slide No. 8).

optimization technique to find the best cluster partition. The program has to be run several times until it converges.

It was first applied to flat field corrected data, 34 bands from 2.0 to 2.34. The classes obtained were seen to be separated according to brightness (Figure 14). For example class 3 is composed of samples having a low DN value in every band. Class 3 and 4 or 2 and 5 would be considered the same by a spectroanalyst.

Several other tries were attempted using data preprocessed to enhance absorption features: ratios, combination of ratios, residuals, normalized data, etc.

No improvement appeared, meaning that the algorithm is not appropriate for "pattern recognition" of absorption features.

V. FIELD CHECKING

Spectra obtained locally were checked by collecting representative samples in the field. Each sample was analysed in lab using:

- PIDAS under artificial vertical illumination;
- the Beckman UV5240;
- XRD technique to get a precise mineralogic composition of non-obvious samples.

A representative spectrum for each outcrop was obtained by averaging the spectra of its samples; it was then compared to the AVIRIS spectrum of the same region. Some problems can be noticed on PIDAS spectra. They are mainly related to grating position and the fact that the samples were not covering the entire field of view of the instrument. Some of the black velvet background is included, causing the jump between the visible and the NIR for example.

In most cases, a good correlation was found as shown on Figure 15. Analysis of mixed area was attempted using Beckman and XRD information. One simple example is shown on Figure 16 where mainly Alunite, Kaolinite and iron oxides are combined. A more detailed study will be published later.

VI. CONCLUSIONS

In conclusion, we can say that despite the engineering problems, some spectral information is present in this data set. Field checking showed a good correlation between spectra obtained on lab from samples and AVIRIS spectra.

No mapping of hydrothermal alteration could be done despite significant efforts mainly because of signal-to-noise performances not good enough and the lack of appropriate software at that time.

An increase in signal-to-noise performances of the instrument, specially in spectrometer D and modification of the SPAM software should allow mapping of alteration areas. This test demonstrates however the potential of high resolution imaging spectrometers for alteration mapping and identification of mineralogy.

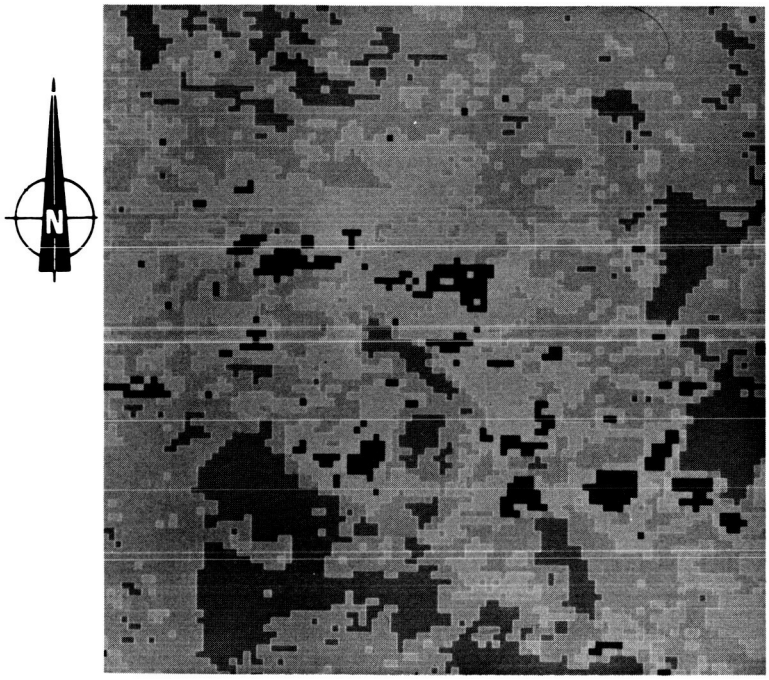

A

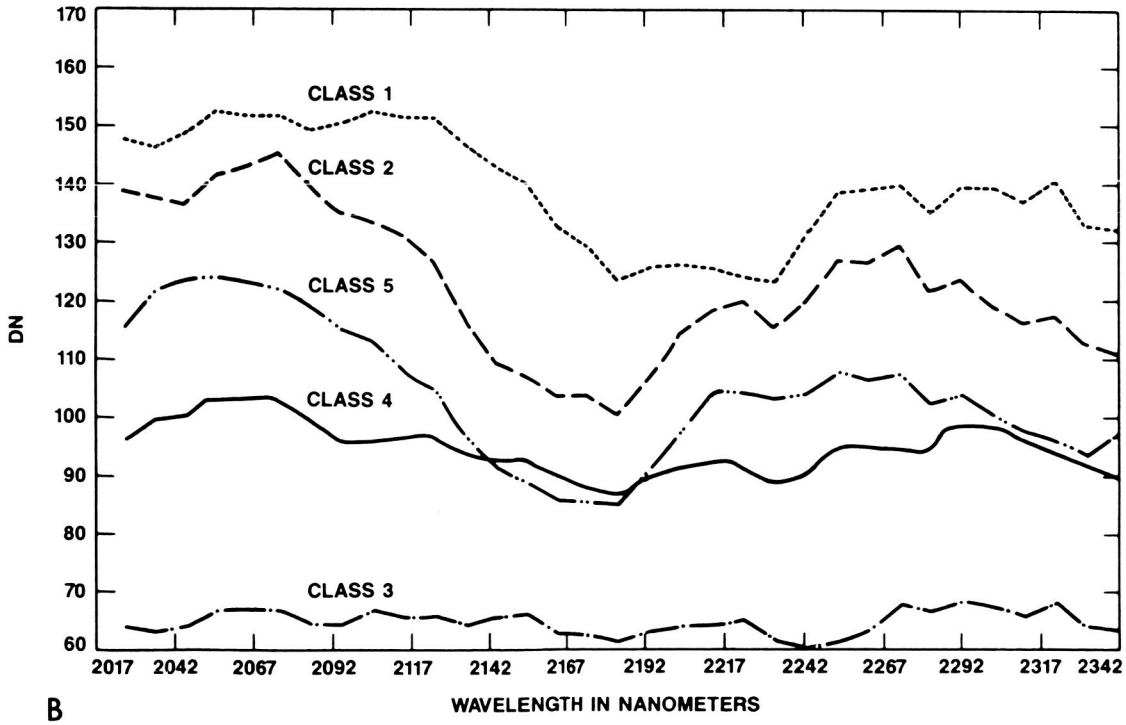

B

Figure 14: A: Classified image obtained using the clustering program CLUSAN (refer to slide No. 9); B: Examples of classes as determined by CLUSAN

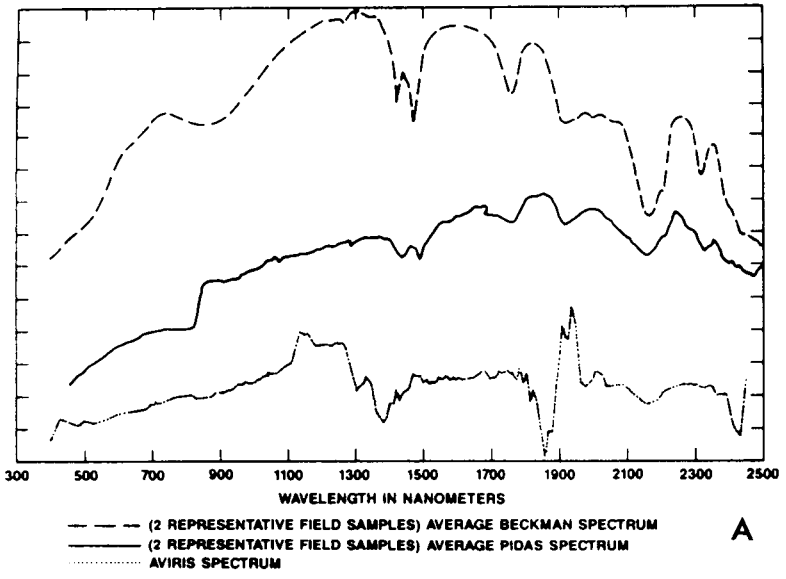

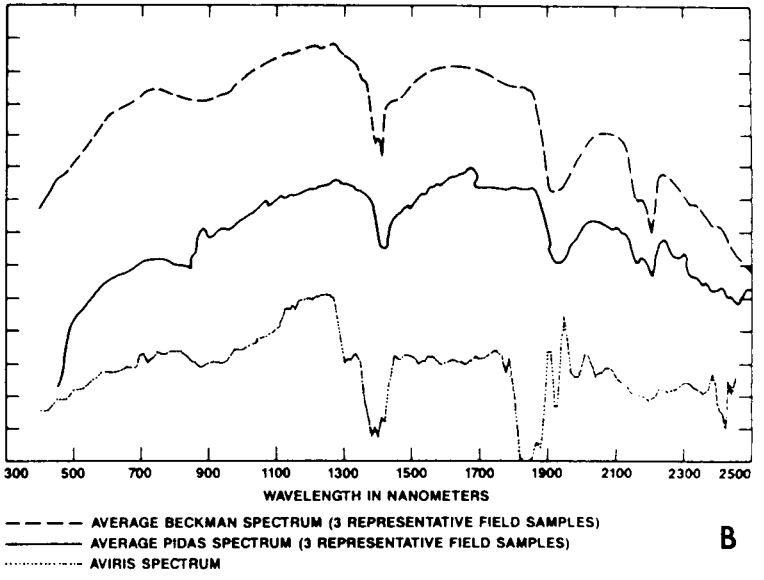

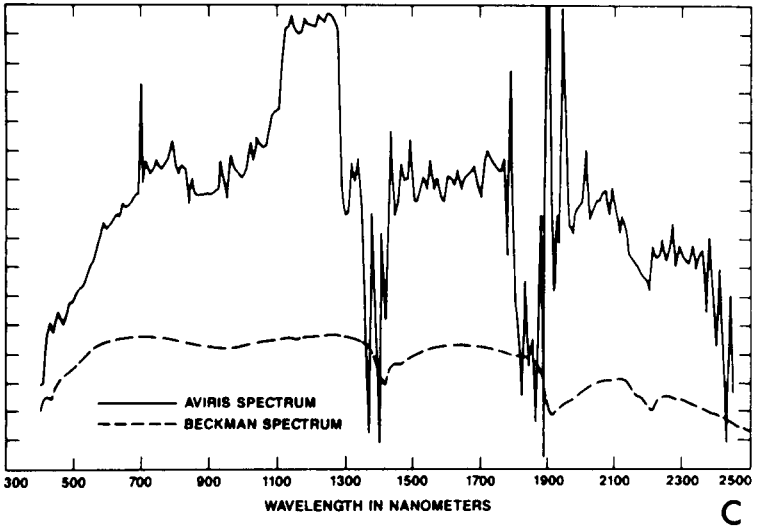

FIGURE 15. Examples of AVIRIS, PIDAS and Beckman spectra for 3 outcrops.

A: outcrop 9 (mainly Alunite)
B: outcrop 13 (mainly Kaolinite)
C: outcrop 15 (mainly Jarosite)

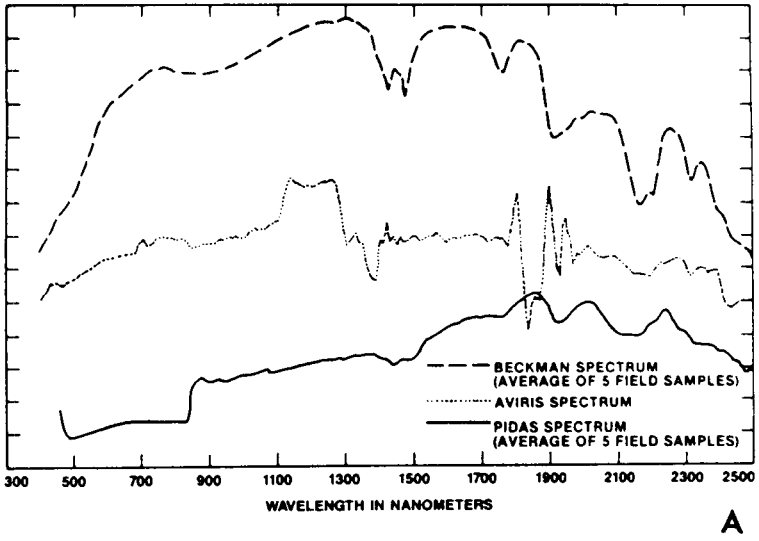

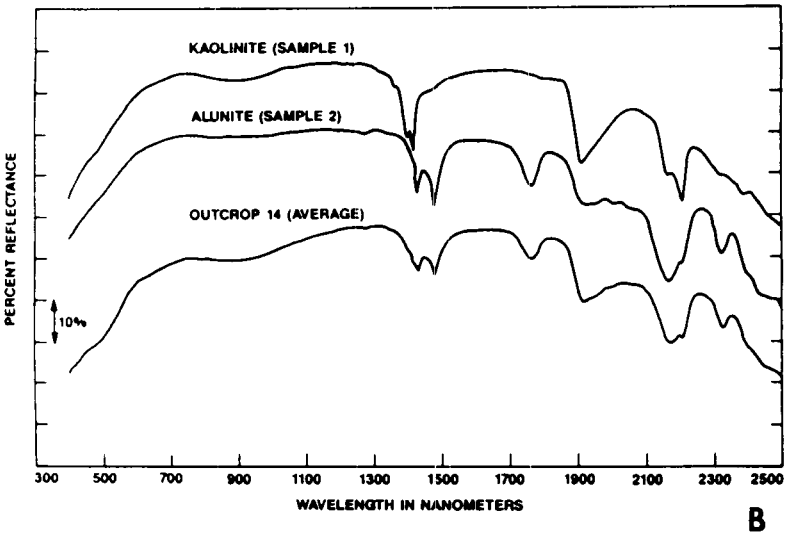

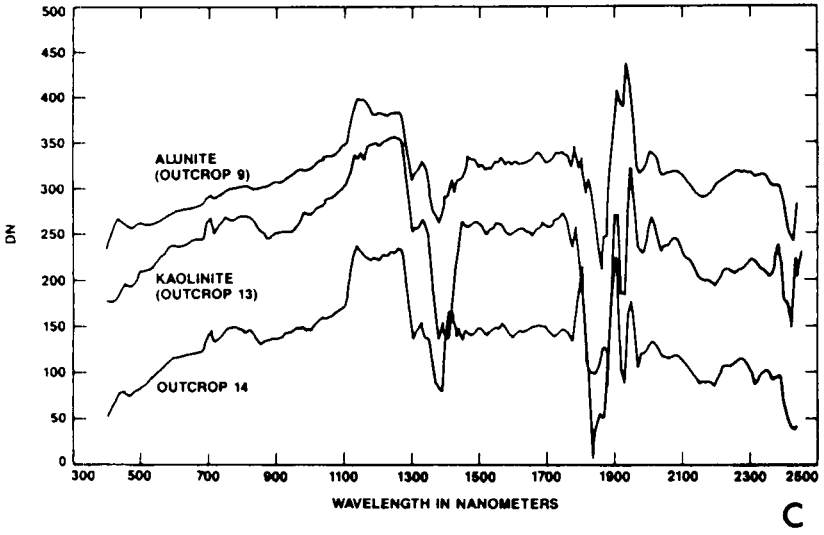

FIGURE 16: Example of mixed area.
A: outcrop 14 - Beckman, PIDAS and AVIRIS spectra;
B: Combination of Kaolinite and Alunite (Beckman spectra from field samples of outcrop 14):
C: Combination of Kaolinite and Alunite (AVIRIS spectra).

REFERENCES

Ashley, R. P. 1972. Premineralization structural history of the Goldfield volcanic center, Nevada. Econ. Geology, v.67, p.1002.

Ashley, R. P. 1974. Goldfield Mining District. In Guidebook to the Geology of four tertiary volcanic centers in central Nevada, Nevada Bur. Mines and Geology Rept 19, p49-66.

Ashley, R. P. and Albers, J. P. 1975. Distribution of gold and other ore-related elements near ore-bodies in the oxidized zone at Goldfield, Nevada. U.S. Geol. Survey Prof. Paper 843-A, 48p.

Ashley, R. P. and Silbermann, M. L. 1976. Direct dating of mineralization of Goldfield, Nevada, by Potassium-Argon and fission-track methods. Econ. Geology, vol. 71, p904-924.

Chrien, T. 1988. AVIRIS laboratory calibration status. Proceedings of the AVIRIS performance evaluation Workshop, this publication.

Conel, J. E., Green, R. O., Vane, G., Bruegge, C. J., Alley, R. E. and Curtiss, B. J. 1987. Airborne Imaging Spectrometer 2, Radiometric and spectral characteristics, and comparison of ways to compensate for the atmosphere. SPIE 834, Imaging Spectroscopy II, 140-157.

Cornwall, H. H. 1972. Geology and mineral deposits of southern Nye County, Nevada. Nevada Bureau of Mines and Geology, Bull. 77, Mackay School of Mines, University of Nevada, Reno.

Green, R.O. and Vane, G. 1988. Inflight determination of AVIRIS spectral calibration using atmospheric gas and surface neodynium absorptions in the vicinity of Mountain Pass, California. Proceedings of the AVIRIS performance evaluation Workshop, this publication.

Harvey, R. D. and Vitiliano, C. J. 1964. Wall-rock alteration in the Goldfield District, Nevada. Jour. Geology, v. 72, p564-579.

Noble, D. C., Anderson, R. E., Ekren, E. B. and O'Connor J. T. 1964. Thirsty Canyon Tuff of Nye and Esmeralda Counties, Nevada. In Geological Survey Research, USGS Prof. Paper 475-D, pD24-D27.

Ransome, F. L. 1909. Geology and ore deposits of Goldfield, Nevada. USGS Prof. Paper 66, 258p.

Reimer, J. 1988. AVIRIS ground data processing. Proceedings of the AVIRIS performance evaluation Workshop, this publication.

Steinkraus, R. E. and Hickok, R. 1987. AVIRIS on-board data handling and control. In Airborne Visible/Infrared Imaging spectrometer (AVIRIS). A description of the sendor, ground data processing facility, laboratory calibration and first results, JPL pub-87-38, Gregg Vane Ed., p.52-60.

Silbermann, M. L. and Mac Kee, E. H. 1972. Summary of radiometric age determinations on Tertiary volcanic rocks from Nevada and eastern California: part. II, western Nevada, Isochron/West n. 4, p7-28.